Fast Radiation Mapping and Multiple Source Localization Using Topographic Contour Map and Incremental Density Estimation

Abdullah Al Redwan Newaz[1], Sungmoon Jeong[1], Hosun Lee[1], Hyejeong Ryu[1], Nak Young Chong[1,2], and Matthew T. Mason[2]

***Abstract*— Toward a global picture of the radiation exposure of an area, particularly for fast emergency response, a UAV based exploration method is proposed. Without *a priori* knowledge of the radiation field, it is difficult to select the region of interest (ROI) which includes all radiation sources. For the case of a single radiation source, a greedy algorithm may localize the source by finding the maximum radiation value. However, when multiple sources generate a hotspot in a cumulative manner, the hotspot position does not coincide with one of the source positions. Therefore, we propose an efficient exploration method to quickly localize the radiation sources using the following procedures: (1) ROI selection using topographic maps with specific radiation level selection methods and (2) source localization estimating the number of sources and their positions with incremental variational Bayes inference of Gaussian mixtures. Under three different conditions according to the number of sources and their positions, we have shown that the proposed model can reduce the ROI and significantly improve the estimation accuracy than existing methods.**

I. Introduction

In disaster recovery planning after a nuclear accident, it is important to know the distribution of radiation levels over contaminated areas so that rescue missions could be accelerated to minimize the losses. In this kind of situation, autonomous flying robots such as Unmanned Air Vehicles (UAVs) can be deployed to monitor the state of radiation effect. The intensity of radiation follows an inverse square relationship as a function of the distance. A radiation field can be characterized by the unimodal Gaussian model if the field contains a collection of sources widely separated from one another [1], [2]. The distribution of sources is then obtained with some form of UAV exploration.

However, if the cumulative radiating effect of sources exists, the field turns out to be complex to estimate, and the sources are no longer at the center of each distribution. Accordingly, the hotspot, where the radiation intensity is maximum, does not coincide with the positions of sources. Therefore, an appropriate model is needed to characterize such a field. Furthermore, UAVs encounter difficulties when exploring a large area with limited resources, *e.g.*, limited battery life and sensing range. Thus, an efficient exploration within a limited fraction of areas should be designed. It is important to estimate the distribution of radiation intensity on the geographic map so that we can reduce our region of interest (ROI) not only for field characterization but also for source localization. In this paper, given the hotspot location along with limited samples of the radiation field, our aim is to localize all radiation sources in a temporally invariant radiation environment.

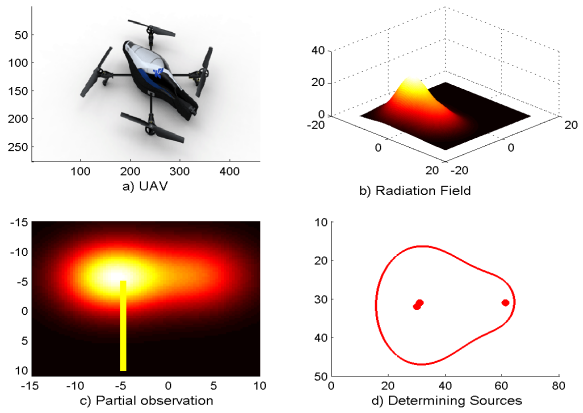

Fig. 1: **Motivation:** UAV explores a radiation field **(a, b)**. With a partial map (yellow line and corresponding measurement) **(c)**, it determines **ROI** (red line) and sources (red dots) **(d)**. The measurement is indicated by colored bands **(b, c)**.

In contrast to earlier exhaustive search based source seeking algorithms [2], [3], we show how to reduce ROI and improve the accuracy of source localization. Radiation sources can be localized using either the Hough transformation (HT) [2] or Gaussian mixture models (GMM) [3]. Since HT utilizes the geometric shape of the contour, if multiple sources are located within close proximity, it considers them a single source, resulting in large localization errors. GMM leads to an accurate estimate of the source position when the number of sources are known, which is usually not possible in unknown radiation fields. We therefore propose the incremental density estimation method that automatically determines the number of components (sources), mean, and variance. Furthermore, the proposed estimation method improves the accuracy of source localization compared to HT. The main contributions of this paper are to answer the following questions.

1) *How to classify the radiation field into a finite number of bands?*
2) *How to find **ROI** in the field?*
3) *How to localize multiple sources within **ROI**?*

[1]School of Information Science, Japan Advanced Institute of Science and Technology, Ishikawa 923-1292 Japan. {redwan, jeongsm, Hosun_LEE, hjryu, nakyoung}@jaist.ac.jp

[2]School of Computer Science and Robotics Institute, Carnegie Mellon University, Pittsburgh, PA 15213. matt.mason@cs.cmu.edu

The rest of the paper is organized as follows: in Sec. 2, we introduce the related works; in Sec. 3, we describe the field characterization and rough classification based on the partial data; in Sec. 4, we present a complete geographical classification based on the local sensing and our strategy to find ROI. In Sec. 5, we explain the proposed source location algorithm. Finally, in Sec. 6 and 7, we present experimental results and draw our conclusion.

II. Related Work

The radiation field can be considered as the mixture of sources. Earlier works dealt only with widely separated sources [1], [2], [4]. Recent studies have made progress in predicting the radiation field with multiple sources using Gaussian Processes [5], [6]. Although several strategies tried to find the radiation hotspot [1], [7], [8], the source positions were difficult to localize when multiple sources exist in an area [3], [9], [10]. Those strategies are mostly divided into model-free and model-based approaches. In the absence of *a priori* knowledge, model-free approaches are basically extremum seeking methods, where the gradient ascending or the maximum likelihood path is followed. Thus, without a pre-specified threshold of the hotspot, those algorithms tend to converge to local maxima [10], [11], [12]. In the context of model-based approach, source seeking can be performed using either the mutual information (MI) [11], [13] or MI gradient [14], [15].

A radiation map can be represented as an intensity grid that could have a finite number of rectangular cells [16]. One can also represent the radiation field using a topographic map [7], [17] whereby the field is characterized by large scale intensity measurements and quantitative representation of distribution with contour lines.

Several search strategies have introduced in literature to estimate the radiation sources. The Archimedian spiral search pattern [18] is basically an exhaustive search within the area of interest. The artificial potential field based exploration [8] might get confused easily with the presence of multiple sources. Multi-robot adaptive sampling classified the radiation field via recursive geometric sub-division [19]. If the area map is known *a priori*, seveal existing methods such as the submodular optimization [20], mutual information gain [21], and maximum entropy based path planning [22] yielded good results.

In the sensor network literature, Chin *et. al.* [23] proposed a hybrid formulation of particle filter and mean shift technique to localize multiple sources. GMM is well-suited for the joint effects of multiple sources [3], [24]. Considering the fixed number of sources, the expectation maximization algorithm was used to estimate the component parameters [9], [23]. If the number of sources are unknown, additional algorithms such as Akaikes information or Bayesian Information Criterion were used to estimate them [24]. Note that measurements of the whole field were available in sensor networks, whereas in our case, the UAV has to gather them with the cost of exploration.

We therefore propose an efficient path planning algorithm for a UAV to localize multiple sources. First, a topographic mapping represents the radiation field with a finite number of contour lines. Few efforts have been made to improve radiation source detection using topographic mapping. Towler *et. al.* [7] used Archimedian spiral search patterns to gather measurement, discovered contour lines with the user defined intensity value, and proposed a HT based approach to estimate the source position. Secondly, we adapt GMM to characterize the radiation field. Finally, we design a novel kernel function for the incremental density estimation algorithm with the Variational Bayesian (VB) framework to automatically estimate the number of sources and their corresponding positions, while limiting computational costs for real time applications.

Fig. 2 shows all the necessary steps of our proposed algorithm. From a given partial map, we find a set of interested measurements (intensity values) coupled with the position information using the log gradient classifier. Starting with initial positions, multiple contour lines are generated by tracking the intensity values. The ROI contour line is then automatically chosen by the contour shape analysis. We limit the UAV exploration for gathering measurements only to the area bounded by the ROI contour. Lastly, we propose a VB algorithm to localize multiple sources accurately.

III. Radiation Field Modelling

We aim to include the distribution of radiation intensity [16] on the geographic map, assuming that the UAV self-localization error is negligible. In this radiation mapping problem, only a partial sample of the field is available observing a UAV trajectory coupled with measurement attributes. It is necessary that the UAV trajectory connects an arbitrary lower intensity zone to the hotspot so that a rough estimation of the radiation field can be made. Toward an efficient and effective mapping method considering the limited resources of UAVs, we categorize the field so that the UAV does not need to visit all the areas, but rather exploring the ROI area to localize the sources.

In this section, we first characterize the radiation field using GMM, and explain how to incorporate prior knowledge. Note that UAV exploration in the ROI area is mandatory, because we cannot determine the parameters of GMM without having real measurement attributes of the field.

A. Field characterization

The intensity in the field could change gradually or abruptly depending on the source location. A region could have high intensity values due to the influence of multiple sources or the presence of strong nearby sources. Hence, it is not possible to detect individual sources with unknown diffusion information about each source. In order to predict their location, we attempt to show their effect in the geographic map, adding the distribution of radioactive intensity on the map. In other words, the cumulative radiation effect of the sources is unlikely to be represented using a unimodal Gaussian model. For this reason we use GMM to characterize

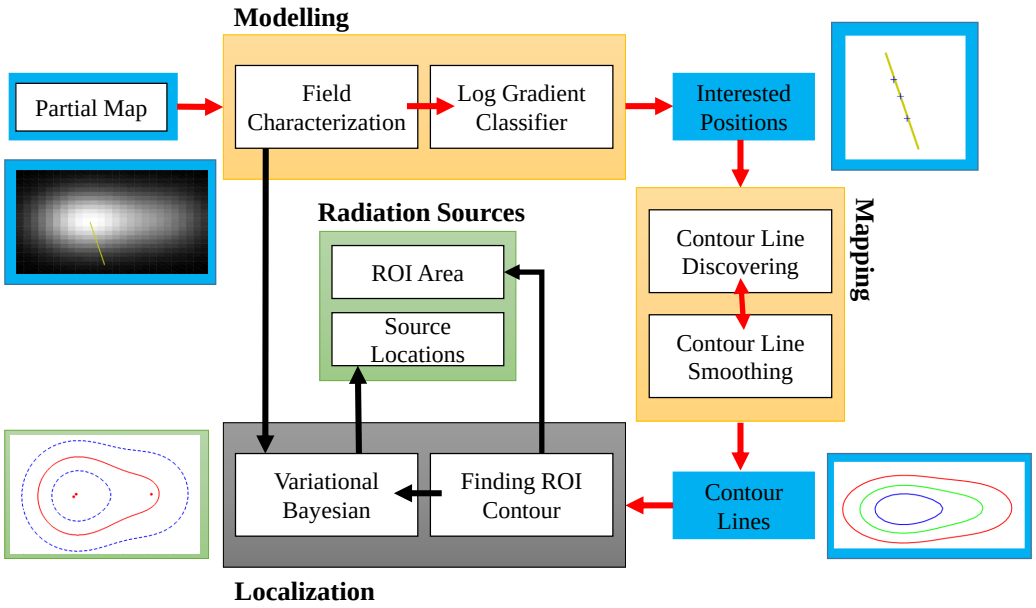

Fig. 2: **System Overview:** A hotspot directed path coupled with measurement is considered as a partial map denoted by the yellow line. The classifier segments the partial observation into a finite number of interested positions denoted by (+) symbols. Topographic mapping generates contour lines from the starting positions assigned by the classifier. UAV chooses **ROI** further explored to determine the source locations. The blue boxes are the output of each process. The yellow boxes and red arrows are the processes for **ROI** selection. The gray box and black arrows are the processes for source localization.

the radiation field. Let $x \in \mathbf{X}$ represent the location of the field and $z(x) \in \mathbf{Z}$ the corresponding measurement. The field property is characterized using GMM with M components such that

$$F_m(x;\alpha,\mu,\sigma) := \sum_{j=1}^{M} \frac{\alpha_j \phi(x-\mu_j)}{{\sigma_j}^2}, \tag{1}$$

where $\phi(x) = \exp\left(-\frac{||x||^2}{2}\right)/(2\pi)$; $\mu_1, ..., \mu_M$ are the means; $\sigma_1, ..., \sigma_M$ are the variances; and $\alpha_1, ..., \alpha_M$ are the mixing weights that describe the Gaussian components. The mixing weights are non-negative and added up to one. In order to generate the ground truth, we assume that each component has equal strength and the relative distance between each mean and measured location has influenced α. However, in our case α is equally divided by the number of sources (M), and the variance (σ) is not important to localize sources. Therefore, we only estimate the mean (μ) of the sources using VB.

B. Log-gradient classifier

The log-gradient classifier (*lgc*) works like a rounding function, converting the partial map into a finite number of interested positions based on the numerical relationship. Let $x_{i=0}$ be the UAV initial position and $x_{i=h}$ indicate the hotspot location. Also let the function $z(x_0, x_i)$ be the relative measurement attribute of the location x_i *w.r.t.* x_0 such that $z : \mathbb{R}^2 \to \mathbb{R}$. Let us draw a line as shown in Fig. 1(c) connecting the UAV location to the hotspot location. The line also contains the measurement attributes of the region traversed by the UAV. Therefore, the partial map is a small fraction of the field including the corresponding measurement attribute. Our target is to group the partial map in an efficient way. First, we investigate how the measurement varies *w.r.t.* the UAV position by taking the gradient at exploration index i given by

$$\nabla_i = \frac{z(x_0, x_i)}{d(x_0, x_i)}, \tag{2}$$

where $d(x_0, x_i)$ is the distance function *w.r.t.* the initial position of the UAV. In order to group the different zones into the same layer, we rather focus on the power of gradient values given by

$$\log(\nabla_i) = \log\left(\frac{z(x_0, x_i)}{d(x_0, x_i)}\right). \tag{3}$$

The log-gradient operator classifies the partial map using Eqn. (3), which depends on the precision value, Λ, to get the number of classified regions x_i^j, where $j \subset i$. In short, the *lgc* takes the set of explored locations, X, and the user defined precision value Λ as the inputs to yield the set of classified regions x_i^j which is basically an $n \times 3$ matrix.

$$\text{lgc}(z(\chi), \Lambda) := \bigcap_{j \subset i}^{n} \left\{ z\left(x_i^j\right), x_i^j \right\} \tag{4}$$

Intuitively, if Λ is a high value, the number of contour lines would increase.

IV. Topographic Mapping

Based on the initially assigned positions by the *lgc*, the whole contour lines are discovered in the contour generation

phase. We use the intensity information to track the contour line. Since the intensity along the contour line is a constant value, the UAV follows the contour line by reducing the measurement error in the intensity domain. However, this kind of contour following algorithms gives fluctuations which are required to be smoothed out, before the analyzing phase starts. In this section, we explain the contour detection and smoothing phases. Note that we start to generate contours radially outward from the hotspot.

A. Contour line discovering

In the contour discovering phase, we draw a contour line enclosing the hotspot, x_h. Thus, the UAV position coordinates are transformed from the global coordinates to a local coordinate system whose origin is x_h. Specifically, we use the polar coordinate system to describe the UAV position. Let r be the Euclidean distance between x_h and a classifier region, say x_c^1. Also let $\delta\theta \in \theta$ be a constant angle of increment in the range $[0 \rightarrow 2\pi]$ and δr be the unit arc length *w.r.t.* $\delta\theta$. If $r(\theta)$ remains equal to r along the whole contour line, it is obvious that the UAV draws a circle from the center x_h. The contour length in the geographic domain, $\mathcal{C}_r$, can be derived using the following equation.

$$C_r = \int_0^{2\pi} r^2 + \left(\frac{\delta r}{\delta\theta}\right)^2 \delta\theta. \tag{5}$$

The value of $r(\theta)$ changes at each exploration step in order to track the assigned intensity I. We now compute the contour length $\mathcal{C}_I$ in the intensity domain such that

$$C_I = \int_0^{2\pi} I^2 + \left(\frac{\delta I}{\delta\theta}\right)^2 \delta\theta, \tag{6}$$

where δI is the difference in the intensity domain. Let the function f map the intensity error such that $f : \delta I \rightarrow \delta r$. One can argue that f may not linearly map the errors. Therefore, to find the gradient in geographic radius, $\nabla r \triangleq \frac{\delta r}{\delta\theta}$, at each exploration step, we adjust $r(\theta)$ in such a way that $\frac{\delta I}{\delta\theta}$ is minimized.

$$\nabla r = \arg\min_{a \in A} E\left\{r(\theta), f(\delta I)\right\}, \tag{7}$$

where a is the opted action among the set A in Eqn. (7). After that, the contour radius is updated as follows

$$r = r + \nabla r. \tag{8}$$

B. Contour line smoothing

Typically, a contour line needs to be smoothed out after the contour discovering process. For instance, $\delta\theta$ in Eqn. (5) is assumed to be a constant value. Then, a quadratic spline interpolation is carried out to smooth the explored line. However, numerical smoothing methods do not take account of actual measurements. Limiting the exploration over the detection process might not be able to represent the true shape of the line *w.r.t.* the field intensity. Therefore, we adaptively adjust the value $\delta\theta$ while exploring the contour line. Let us assume that $\exists(\delta\theta)$ for which δI is large. We take more measurements in such a way that the current contour radius $r(\theta)$ adaptively controls the step increment given by

$$\delta\theta^* = \delta\theta\left(\cot^{-1}\left(\sqrt{\frac{\delta I^2}{\delta\theta^2}}\right)\right). \tag{9}$$

It is obvious from the above equation that $\delta\theta^*$ asymptotically decreases for a larger δI, resulting in increased UAV exploration. Thus, a sudden change of intensity cannot cause the UAV to deviate significantly from the contour line.

C. Finding the ROI contour

A topographic map may contain multiple contour lines depending on the precision value (Λ) of the classifier. However, all the contour lines are not important to explain the characteristic property of distribution. Obviously, contours near to the hotspot region are very important, since they incorporate the most vital information on the field. As the contour goes outwards from the hotspot, the shape tends to be quite similar to each other. Therefore, we can analyze the contours shape that allows the UAV to terminate the exploration. From the contour line discovering process, we can find $C_l = \{C_1, C_2, ..., C_n\}$, where C_l is the set of all contour lines, C_r is the length of each contour, and n is the number of contour lines. Also note that C_I represents the intensity of the contour. In order to measure the degree of similarity between neighboring contour lines, we introduce the elements σ_x and σ_y, at each contour discovering process. We now compute the relative changes of initially assigned radius, r_a, to the radius, r, at the current exploration step such that

$$\begin{aligned} \sigma_x &= \left\{(r - r_a)\cos(\delta\theta)\right\}, \\ \sigma_y &= \left\{(r - r_a)\sin(\delta\theta)\right\}. \end{aligned} \tag{10}$$

It is obvious from the above equation that $\hat{\boldsymbol{\sigma x}} = \left\{\bigcup_i {\sigma_x}^i\right\}$ and $\hat{\boldsymbol{\sigma y}} = \left\{\bigcup_i {\sigma_y}^i\right\}$ represent the change in the radius *w.r.t.* the global Cartesian x-axis and y-axis, respectively. Next, we will analyze the similarity between two neighboring contour lines by defining a function given by $\lambda : \mathbb{R}^n \rightarrow \mathbb{R}$. We compute a score for each contour line *w.r.t.* the neighboring contour line closer to the hotspot using the following equation

$$\lambda^* = \tan^{-1}\frac{E\{\hat{\boldsymbol{\sigma x}}\}^2}{E\{\hat{\boldsymbol{\sigma y}}\}^2} - \lambda, \tag{11}$$

where λ^* is the current contour score and λ is the neighboring contour score. When λ^* reaches a predefined tolerance limit, adding a new contour would be redundant. Therefore, the UAV can stop its exploration and narrow down ROI to the previous contour such that

$$\arg\min_n \left\{\max_{\lambda^* \in \lambda^n} \left\{\lambda^n(C_n, C_{n-1})\right\}\right\}. \tag{12}$$

V. Radiation Source Localization

Although we have gathered the measurement attribute by sampling the ROI area $\bar{\mathbf{Z}} \subset (Z)$, the actual sources $\bar{\mathbf{X}} \subset (X)$ are hidden variables. We now find the maximum likelihood estimate of the parameters of $\bar{\mathbf{X}}$. Assuming that we have no prior distribution, the optimal number of components for Bayesian GMM can be obtained iteratively using a variational EM algorithm [25]. This is achieved through partially performing an E-step and observing the maximization of E-step and M-step using the same function $F[q, \pi]$ such that

$$F\left[q, \pi\right] = \sum_{x \in \bar{X}} \int q\left(\bar{Z}, \mu, \mathrm{T}\right) \log \frac{p\left(\bar{X}, \bar{Z}, \mu, T; \pi\right)}{q\left(\bar{Z}, \mu, \mathrm{T}\right)} \partial\mu \partial T, \tag{13}$$

where the parameters (μ, T, π) are the mean (center) of the sources, the precision matrices, and the mixture weights, respectively. q is the arbitrary distribution that approximates the posterior distribution $p\left(\bar{X}, \bar{Z}, \mu, T; \pi\right) \overset{def}{=} p\left(\bar{X} | \bar{Z}, \mu, T | \bar{X}; \pi\right)$. We prepare the input vector for the Bayesian model as follow.

$$p(\bar{X}|\bar{Z}) = \mathcal{N}(\bar{X}, \mu) - k(\bar{Z}), \tag{14}$$

where k is the kernel used to bias the location inputs based on the magnitude of measurement such that

$$k(\bar{Z}) = \frac{1}{2 + \exp(\bar{Z})}. \tag{15}$$

From Eqn. (14), we can see that uniform samples inside the ROI are explicitly biased toward the significant measurement attribute, which results in conversion of cluster samples. Therefore, VB can easily estimate the optimal number of sources and their corresponding locations. The detailed formulas for computing the parameters can be found in [25]. At each iteration, VB performs the following two steps:

- **Variational E-Step:** Evaluate $q^* = \arg\max_{q} F\left[q, \pi\right]$
- **Variational M-Step:** Find $\pi^* = \arg\max_{\pi} F\left[q^*, \pi\right]$

A notable property of this model is that when maximizing F, the prior distribution of μ and T penalize the overlapping components, therefore the redundant sources whose effect is negligible to the distribution are eliminated. Furthermore, it is sufficient to find the mean μ components to estimate the source position.

VI. Simulation Result

We have performed an extensive simulation validation of our algorithm in the different settings of the sources. Our first experiment focuses on reducing ROI depending on measurement distribution. Next, we demonstrate the source localization strategy. The partial map given does not depend on specific initial positions. It just contains the rough idea of the intensity distribution from lower to higher zones.

A. Reducing ROI

The partial map of the environment contains the UAV trajectory and corresponding measurement up to the hotspot location. The *lgc* classifies the trajectory depending on the measurement change. The main advantage of *lgc* is that it automatically segments the trajectory depending on the numerical properties of the measurement, resulting in a finite number of groups. Each group contains the starting position and the corresponding measurement value. It is then further explored to determine the whole line through the contour discovering process. We perform three experiments for the scattered, clustered, and biased source cases, respectively.

Fig. 3 represents our experimental results, where the contour lines are drawn by mapping the intensity changes into the geographic domain. The background gray colored map is the distribution of the measurement, while the yellow line represents the partial map that is fed to *lgc*. Although *lgc* segmented the field into a finite number of groups, the similarity analysis of contour shape allow us to reduce the ROI further more. The similarity slope varies depending on the distribution. As can be seen in Fig. 3 (c), (g), (k), the similarity slope between two consecutive contours reaches a saturation level after a certain period. When the slope gets saturated, we can discard the current contour and fix our ROI onto the previous one, which explains why the ROI contours in Fig. 3 (d), (h), (l), are $2, 1, 2$, respectively.

B. Source localization

We have extended our experiment to source localization. Fig. 4 shows the overall procedure, where the partial map in Fig. 3 (i) is discretized using the *lgc* to generate a finite number of contours. Among the contours, the ROI contour is selected for further exploration whereby uniformly spaced samples are taken denoted by the red circles in Fig. 4 (b), (e), (h). It can be seen from Fig. 4 (a), (d), (g) that the area bounded by the initial contours was approximately $30m \times 25m$, while the ROI was at most $15m \times 15m$, showing a significant reduction in exploration area size.

The localization accuracy of VB and HT was assessed by the distance between the actual sources and the nearest estimated source given by NDS1, NDS2, and NDS3, respectively in Table I. In Fig. 4 (c), (f), (i), the red dots are the actual sources, while the black and green circles are the estimates using HT and VB, respectively. The performance of VB is outstanding and very close to the actual source location. VB takes at most 264 iterations to converge to the resulting state with a reduced sample size inside the ROI contour. The worst case estimation error of VB is $4.490m$, while that of HT is $10.837m$.

VII. Conclusion

A UAV exploration based multiple radiation source localization problem was investigated. The log gradient classifier converted the partial map into a set of finite positions. Starting with the assigned positions of the classier, the contour lines were generated by tracking the constant intensity values. The smoothing of a contour line was considered as an

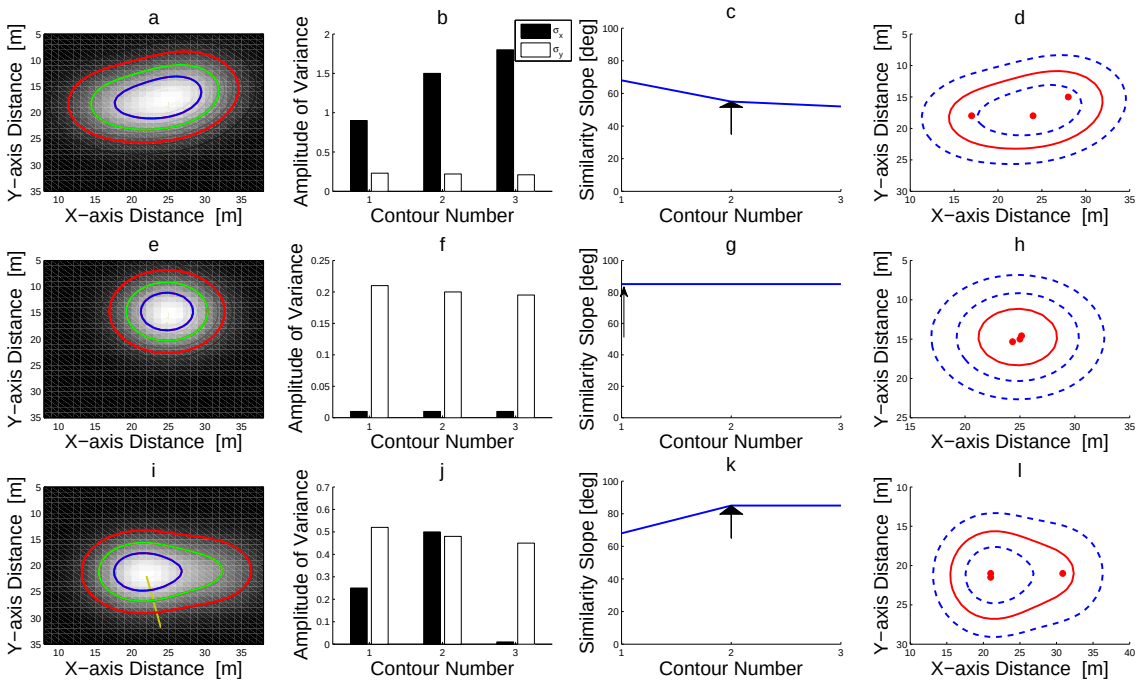

Fig. 3: **Finding ROI:** The ROI contour is determined by similarity analysis for three different cases: scattered (a-d), clustered (e-h), and biased sources (i-l). The blue, green, red contours in (a,e,i) are labeled as (1,2,3) in (b, c, f, g, j, k). The variance of each contour is computed over circular path while the similarity slope between two consecutive contours is computed using Eqn. (12). The arrow in (c, g, k) indicates the starting position of similar contours. The red contour line in (d, h, l) represents the ROI contour, where the red dots are the actual sources.

TABLE I: Sources estimation

Src. type	Method	No. Src. (ground truth)	NDS1	NDS2	NDS3
Scatter	Proposed	3 (3)	4.490	2.618	1.942
	Hough	1 (3)	4.490	2.618	7.758
Cluster	Proposed	2 (3)	0.778	1.399	1.604
	Hough	1 (3)	0.778	1.408	1.707
Biased	Proposed	2 (3)	2.570	0.998	2.502
	Hough	1 (3)	10.837	0.998	10.687

online process, where further attentions were given to obtain the measurement attributes from the radiation field.

We have demonstrated that the similarity analysis of the contour lines significantly reduced the ROI. The area bounded by the ROI contour was further explored to gather the measurement attributes. The ROI also reduced the amount of sample locations which were important for source localization. Finally, we proposed a kernel function for VB to localize multiple sources, where the radiation field was characterized as a GMM. It was shown that VB clearly outperformed HT.

Future research will focus on the following issues: (1) *Termination rule of exploration* - The contour discovering process was terminated by a threshold value. The effect of acceptability threshold on the similarity analysis will be considered. (2) *3D exploration*- The proposed 2D planner will be extended to 3D to see how the altitude influences the localization. (3) *Variable source strength*- Since the VB can compute the mixing weights for the sources, the sources with variable strength will be tested in the same manner. (4) *The size of ROI* - If the distribution of the sources was bounded by the limited area, reducing the ROI was reasonably enough to localize the sources. The future work will involve the cost analysis between the required exploration and the localization accuracy. (5) *Real world experiments* - The proposed method will be demonstrated in different fields generated by light, RF, or thermal sources.

REFERENCES

[1] R. Cortez, X. Papageorgiou, H. Tanner, A. Klimenko, K. Borozdin, R. Lumia, and W. Priedhorsky, "Smart radiation sensor management," *IEEE Robotics & Automation Magazine, 15(3):85-93*, 2008.

[2] G. F. Knoll, *Radiation detection and measurement*. John Wiley & Sons, 2010.

[3] M. R. Morelande and A. Skvortsov, "Radiation field estimation using a gaussian mixture," in *Int'l Conf. Information Fusion, 2247-2254*, 2009.

[4] S. Bashyal and G. K. Venayagamoorthy, "Human swarm interaction for radiation source search and localization," in *IEEE Swarm Intelligence Sympo., 1-8*, 2008.

[5] M. Reggente and A. J. Lilienthal, "Using local wind information for gas distribution mapping in outdoor environments with a mobile robot," in *IEEE Sensors, 1715-1720*, 2009.

[6] N. Cao, K. H. Low, and J. M. Dolan, "Multi-robot informative path planning for active sensing of environmental phenomena: A tale of

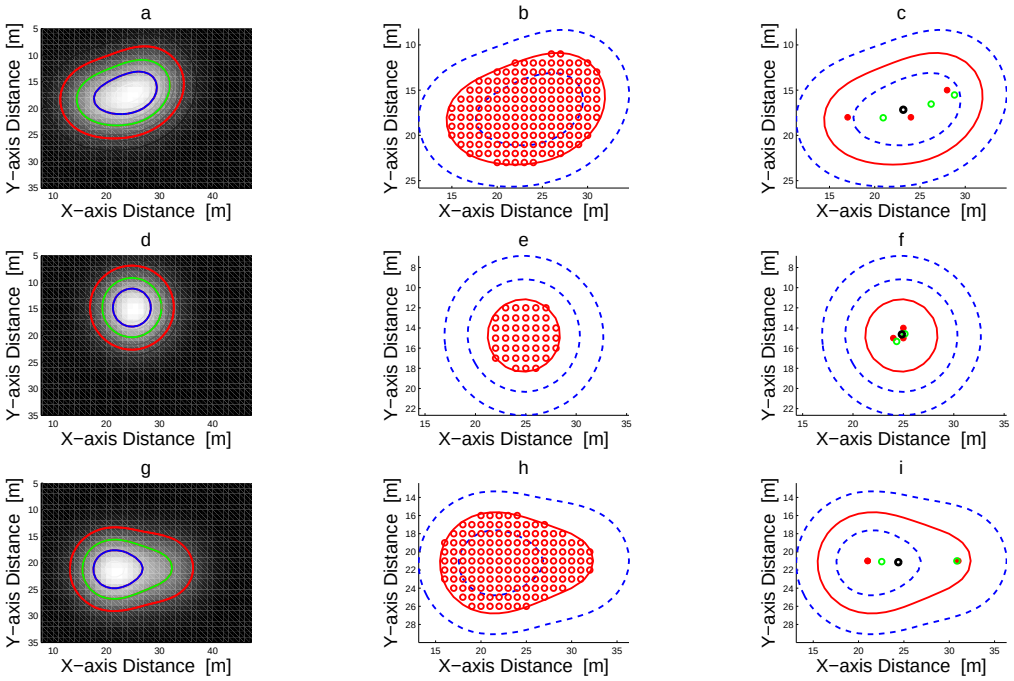

Fig. 4: **Source Localization:** A radiation field is turned into contour lines **(a, d, g)**. Contour generation is terminated depending on similarity in shape analysis and uniform samples are taken inside the ROI **(b, e, h)**. In **(c, f, i)**, red dots are the actual sources, black circles are estimated by Hough transform and green circles by the proposed algorithm.

two algorithms," in *Int'l Conf. Autonomous Agents and Multiagent Systems, 7-14*, 2013.

[7] J. Towler, B. Krawiec, and K. Kochersberger, "Radiation mapping in post-disaster environments using an autonomous helicopter," *Remote Sensing, 1995-2015*, 2012.

[8] A. Gunatilaka, B. Ristic, and R. Gailis, "On localisation of a radiological point source," in *Information, Decision and Control, 236-241*, 2007.

[9] M. Morelande, B. Ristic, and A. Gunatilaka, "Detection and parameter estimation of multiple radioactive sources," in *Int'l Conference Information Fusion, 1-7*, 2007.

[10] E.-W. Bai, K. Yosief, S. Dasgupta, and R. Mudumbai, "The maximum likelihood estimate for radiation source localization: Initializing an iterative search," in *IEEE Conf. Decision and Control, 277-282*, 2014.

[11] B. Charrow, V. Kumar, and N. Michael, "Approximate representations for multi-robot control policies that maximize mutual information," in *Robotics: Science and Systems*, 2013.

[12] E. A. Miller, T. A. White, K. D. Jarman, R. T. Kouzes, J. A. Kulisek, S. M. Robinson, and R. A. Wittman, "Combining radiography and passive measurements for radiological threat localization in cargo," *IEEE Trans. Nuclear Science, 2234-2244*, pp. 2234–2244, 2015.

[13] G. Hitz, A. Gotovos, F. Pomerleau, M.-E. Garneau, C. Pradalier, A. Krause, and R. Y. Siegwart, "Fully autonomous focused exploration for robotic environmental monitoring," in *IEEE Int'l Conf. Robotics and Automation, 2658-2664*, 2014.

[14] C. Wang, C.-Y. Lin, and M. Tomizuka, "Statistical learning algorithms to compensate slow visual feedback for industrial robots," *ASME Jour. Dynamic Systems, Measurement, and Control, 031011*, 2015.

[15] P. Dames, M. Schwager, V. Kumar, and D. Rus, "A decentralized control policy for adaptive information gathering in hazardous environments," in *IEEE Conf. Decision and Control, 2807-2813*, 2012.

[16] R. Cortez and H. Tanner, "Radiation mapping using multiple robots," in *ANS Joint Topical Meeting Emergency Preparedness and Response and Robotic and Remote Systems, 157-159*, 2008.

[17] J. Han and Y. Chen, "Multiple uav formations for cooperative source seeking and contour mapping of a radiative signal field," *Jour. Intelligent & Robotic Systems, 323-332*, 2014.

[18] A. Ghoshal, D. Shell *et al.*, "Covering space with simple robots: from chains to random trees," in *IEEE Int'l Conf. Robotics and Automation, 914-920*, 2013.

[19] Y.-H. Kim and Shell, "Distributed robotic sampling of non-homogeneous spatio-temporal fields via recursive geometric subdivision," in *IEEE Int'l Conf. Robotics and Automation, 557-562*, 2014.

[20] A. Krause and C. Guestrin, "Near-optimal observation selection using submodular functions," in *AAAI Conf. Artificial Intelligence, 1650-1654*, 2007.

[21] K. H. Low, J. M. Dolan, and P. Khosla, "Adaptive multi-robot wide-area exploration and mapping," in *Int'l Conf. Autonomous Agents and Multiagent Systems, 23-30*, 2008.

[22] K. H. Low, J. M. Dolan, and P. K. Khosla, "Information-theoretic approach to efficient adaptive path planning for mobile robotic environmental sensing," in *Int'l Conf. Automated Planning and Scheduling*, 2009.

[23] J.-C. Chin, D. K. Yau, and N. S. Rao, "Efficient and robust localization of multiple radiation sources in complex environments," in *IEEE Int'l Conf. Distributed Computing Systems, 780-789*, 2011.

[24] M. Ding and X. Cheng, "Fault tolerant target tracking in sensor networks," in *ACM Int'l Sympo. Mobile Ad Hoc Networking and Computing, 125-134*, 2009.

[25] D. G. Tzikas, A. C. Likas, and N. P. Galatsanos, "The variational approximation for bayesian inference," *IEEE Signal Processing Magazine, 131-146*, 2008.